Nanoscale

Accepted Manuscript

This article can be cited before page numbers have been issued, to do this please use: V. Russo, N. T. Michieli, T. Cesca, C. Scian, D. Silvestri, M. Morpurgo and G. Mattei, *Nanoscale*, 2017, DOI: 10.1039/C7NR01982C.

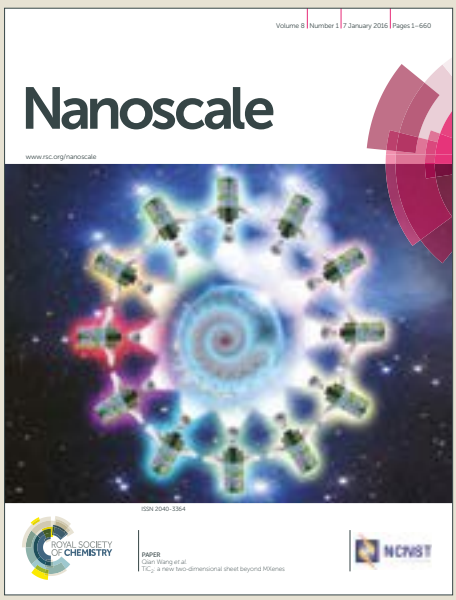

View Article Online
DOI: 10.1039/C7NR01982C

Journal Name

ARTICLE TYPE

Cite this: DOI: 10.1039/xxxxxxxxxx

Gold-silver alloy semi-nanoshell arrays for label-free plasmonic biosensors†

Valentina Russo,[a] Niccolo' Michieli,[a] Tiziana Cesca,*[a] Carlo Scian,[a] Davide Silvestri,[b] Margherita Morpurgo,[b] and Giovanni Mattei*[a]

Received Date
Accepted Date

DOI: 10.1039/xxxxxxxxxx

www.rsc.org/journalname

Nanosphere lithography coupled to reactive ion etching has been used to synthesize hexagonal ordered arrays of Au-Ag bimetallic semi-nanoshells to be used as plasmonic biosensors. The degree of lateral interaction between adjacent semi-nanoshells can be controlled by tailoring the reactive ion etching time in order to boost the global plasmonic properties through the formation of near-field hot-spots, which in turn can improve the sensitivity of the biosensors. To test the efficiency of the proposed system as a biosensor, we used an established protocol for the detection of biomolecules (local sensitivity), based on the receptor-ligand approach and using the Biotin-Streptavidin model system. We also tested the sensitivity to a homogeneous change in the refractive index of the buffer over the sensor (bulk sensitivity). Comparing the obtained results to those of array of nanoprisms, chosen as a benchmark, significantly higher performances both in local and in bulk sensitivity have been found, in agreement with electrodynamic simulations based on finite-element methods.

The interest in using the surface plasmon resonance (SPR) of metal structures to realize sensing devices started in the first years of 1980[1]. SPR sensors are used in many fields including the analysis for food quality[2], for environmental monitoring[3] and for pharmaceutical or medical diagnostics[4–7]. They are based on the excitation of surface plasmon polaritons (SPP) at a metal/dielectric interface. SPP can be subdivided into propagating SPP (PSPP) and localized SPP (LSPP). The localized SPP, in particular, are characterized by a strong field confinement, and this property can be exploited for biosensing. Indeed, in the last twenty years a very intense research activity has been focused on the investigation and the use of noble metal nanoparticles with different shapes to realize devices for biological detection. The sub-wavelength field localization and the consequent strong enhancement is used to boost the interaction between the incident light and the analytes in a limited region around the nanostructures to achieve improved optical sensing either by measuring the shift in the localized surface plasmon resonance (LSPR) or by using Surface Enhancement Raman Spectroscopy (SERS) enhanced signal.[8–16] The principal aim of those studies was to design innovative nanostructures, whose plasmonic properties can be exploited to realize optical biosensors for label-free and high-specificity detection of low concentrations (below the *pM* level) of biomolecules with low molecular weight. The specificity of the detection can be obtained by functionalizing the nanostructures with suitable receptors, which are able to selectively bind the corresponding analyte only. In this way, the desired analyte, and only that one, is confined in the localized field region, so that the enhanced interaction with light is experienced only by the desired analyte. The detection event is characterized by the change in the optical properties of the nanostructures, which, in turn, is due to the change of the refractive index around them as the analytes bind to the receptors. Compared to other types of biosensors, the high sensitivity of LSPP-based confined nanostructures allows to avoid the use of an optical marker, obtaining a label-free detection by measuring the change of the extinction spectrum with simple and cost-effective transmission techniques[7]. Another advantage of the use of these systems is their inherent aptitude to be scaled down to very small sizes, i.e., to sizes comparable to those of biological molecules, such as proteins or nucleic acids. As a consequence, in these cases, they can be exploited even at single-molecule detection level[17].

Generally, the LSPP sensors are based on nanoparticles bound to a substrate rather than in solution, to avoid their intrinsic instability and the aggregation as a consequence of variations of the pH or temperature[7,18]. Many kinds of plasmonic nanosystems have been investigated, such as nanodisks, nanorings[19], nanoholes[20], nanoprisms[21], nanoshells[22–24], nanorods[11,25,26],

[a] University of Padova, Department of Physics and Astronomy, NanoStructures Group, via Marzolo 8, I-35131 Padova, Italy. E-mail: tiziana.cesca@unipd.it, giovanni.mattei@unipd.it
[b] Department of Pharmaceutical and Pharmacological Sciences, University of Padova, via Marzolo 5, I-35131 Padova, Italy.
† Electronic Supplementary Information (ESI) available.

View Article Online
DOI: 10.1039/C7NR01982C

nanogaps[27], nanodots[28], nanocrescent moon structures[13]. One of the most simple, inexpensive and used patterning technique to obtain nanoparticles organized in two-dimensional ordered arrays with high control on size, morphology and composition, is the nanosphere lithography (NSL)[21,29,30]. The main approach to biosensing using NSL over the past years has been based on the fabrication of nanoprism arrays (NPA) as optical transducers[21]. In recent years a new kind of nano-array based on gold semi-nanoshells (SNS), still obtained using NSL, was investigated as SERS substrate[22,31]. Calculations have shown that the gaps between SNS are regions of very intense hot-spots of local-field enhancement.

In this work, we present a modified fabrication method of SNS arrays (SNSA), developed to obtain nanostructures made of an alloy of two metals, Au and Ag in the present case. Owing to its high chemical stability gold is definitely the most used metal for the fabrication of biosensing devices. On the other hand, silver is in general considered a better material from the plasmonic point of view for its reduced losses with respect to Au.[10,32] On the basis of these considerations, we performed Finite Elements Method (FEM) simulations to assess the performances of Au-Ag alloy SNSA, showing that an enhancement of sensitivity is obtained in this case with respect to pure Au SNSA (see the Electronic Supplementary Material†). Here we report the results of our experimental study on the optical and biosensing properties of Au-Ag alloy SNS arrays synthesized by NSL. In particular, the effect of the electromagnetic coupling between the nanostructures on the LSPR response for proteins detection is investigated. The attractive characteristics of the SNS arrays are the high sensitivity to refractive index changes (in particular, in close proximity to their surface), the possibility to have a good control on the structure and as a consequence on the LSPR spectral position, which can be tuned from UV to NIR region, and the stability for device applications.

1 Experimental Section

1.1 Sample preparation

Au-Ag alloy SNS arrays (SNSA) were synthesized by Nanosphere Lithography (NSL)[21]. The process can be divided into three main steps, as illustrated in Fig. 1a. In the first step, a mask of polystyrene (PS) nanospheres is self-assembled on a soda-lime glass substrate. Before the synthesis of the mask, the substrate is cleaned in a piranha solution (3:1 by volume of 30% H_2O_2 and 98% H_2SO_4) for 1 hour at 90 °C and then washed in ultra-pure milliQ water. Commercial polystyrene nanospheres (micro-Particles GmbH) with diameter D = 315 ± 9 nm were used. The second step is a Reactive Ion Etching (RIE) process performed to reduce the initial diameter of the nanospheres and thus opening gaps between them, without altering the array periodicity. RIE treatments were done in an Ar-O_2 atmosphere (60 % Ar and 40 % O_2) at a total pressure of 4×10^{-2} mbar for different time intervals to control the degree of lateral coupling (the measured etching rate for the nanosphere diameter was about 20 nm/min). Two configurations of SNSA were produced, in the following named low-interaction (LI) and high-interaction (HI) SNSA. In the third step, a thin bimetallic layer (equivalent to a 30 nm thick film, which corresponds to a shell thickness of about 20 nm at the nanospheres equator) is deposited on the etched nanospheres by magnetron co-sputtering. Au and Ag depositions were performed at the same time by using two sources, with the same inclination (15 deg) with respect to normal direction of the sample surface. The samples are mounted on a rotating sample-holder. This co-deposition results in a homogeneous Au-Ag alloy layer covering the upper part of the etched PS nanosphere to form the plasmonic SNS, which constitutes the functional building block of the array. As an example, in Fig. 1b we have reported scanning electron microscopy (SEM) images of a typical sample. This method allows to obtain Au-Ag SNS arrays with a high degree of order up to 1 cm^2 size scale.

The choice of fabricating Au-Ag alloy SNSA was motivated by the results on the sensors bulk sensitivity obtained by Finite Elements Method (FEM) simulations, which were performed before the SNSA synthesis and bio-functionalization experiments. Details about the FEM simulations and the obtained results are reported in the ESI†. An enhancement of the bulk sensitivity of more than 20% was obtained for Au-Ag SNSA with respect to pure Au SNSA in the HI configuration (and more than 10% for the LI configuration). Pure Ag was not used, instead, to avoid the possible deterioration of the sensor properties due to surface oxidation and to guarantee its stability over time.

1.2 Bio-functionalization protocol

A schematic illustration of the bio-functionalization protocol of the samples is reported in Fig. 1c. This protocol was developed by Van Duyne's group for the functionalization of NPA[33]. At first, the samples are incubated for 15 h in a thiols solution, 1 mM, of 1-Octanethiol (1-OCT):11-Mercaptoundecanoic acid (11-MUA) in 3:1 ratio in ethanol. This forms a protective layer over the SNSs indicated as the self-assembled monolayer (SAM) in Fig. 1c. Then, the samples are washed with pure ethanol and dried in vacuum for about 30 minutes. The second step is the coupling of the biomolecular receptor (Biotin-PEO_2-Amine) to the SNSs using a 1-Ethyl-3-[3-dimethylaminopropyl]carbodiimide hydrochloride (EDC) cross-linking agent. The EDC activates the carboxyl groups (-COOH) of 11-MUA to bind to the NH_2 groups of the Biotin-PEO_2-Amine, forming an amide bond between the receptor and the thiols layer[34]. For this functionalization, the samples are incubated in a solution 1 mM of Biotin-PEO_2-Amine with 10 mM of EDC in a phosphate-buffered saline (10 mM phosphate, 150 mM NaCl, pH 7.4 - PBS) solution for 3 h. Then, they are washed with PBS 10 mM and ultra-pure water to remove unbound molecules and dried in vacuum.

Finally, for the recognition event between receptor and analyte, the samples are incubated in a solution of Streptavidin (SA) at different concentrations (10^{-13} M $\leq$ [SA] $\leq$ 10^{-6} M) in PBS 10 mM for 5 h to ensure achieving of binding equilibrium, washed with PBS and pure water and dried in a N_2 flux.

1-Octanethiol, 11-Mercaptoundecanoic acid, ethanol, PBS, EDC, Streptavidin and BSA (Albumin from bovine serum) were purchased from Sigma Aldrich while Biotin-PEO_2-Amine was pur-

View Article Online
DOI: 10.1039/C7NR01982C

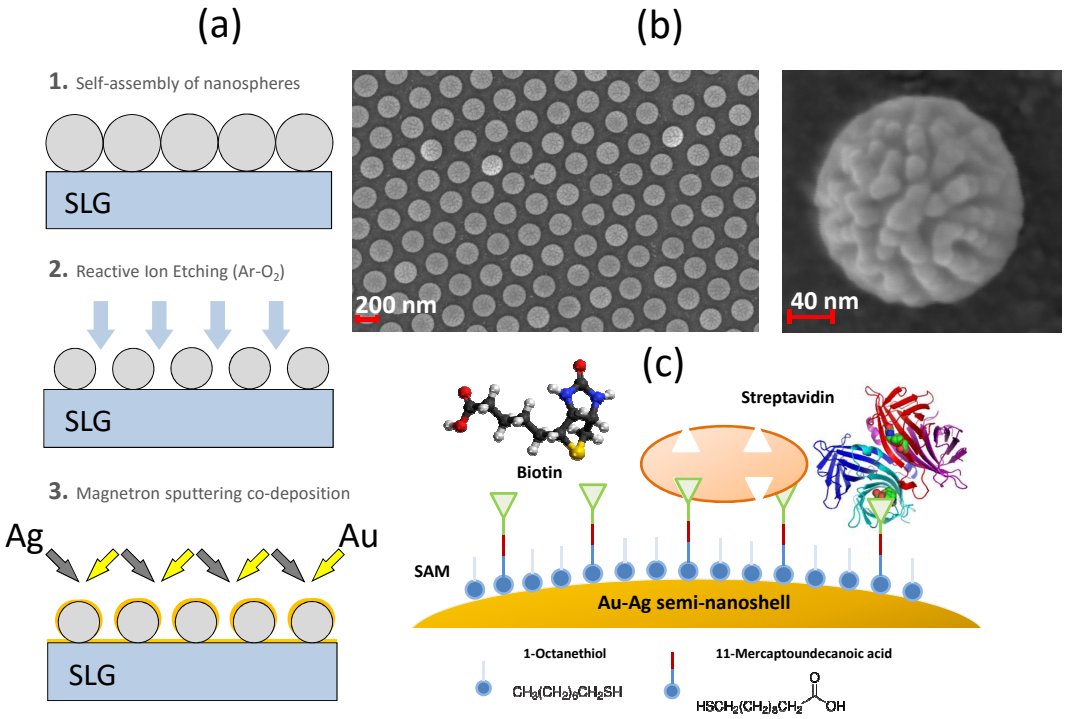

Fig. 1 (a) Schematic diagram of the synthesis process of Au-Ag semi-nanoshells (SNS) arrays: 1) self-assembly of a PS nanospheres mask on a soda-lime glass (SLG) substrate, 2) reduction of PS nanospheres diameter by reactive ion etching, 3) co-deposition of Ag and Au by magnetron sputtering. (b) FE-SEM image of a typical Au-Ag SNS array at different magnification. (c) schematic illustration of the SNS bio-functionalization protocol (not to scale).

chased from Thermo Scientific. All reagents were used without further purification.

1.3 Characterization techniques

The morphological properties of the samples were investigated with field-emission scanning electron microscopy (FE-SEM) and atomic force microscopy (AFM). The FE-SEM microscope utilized is a Zeiss SIGMA HD that can operate in the 0.2–30 kV range, with a spatial resolution of about 1.2 nm at 30 kV. It is equipped with a detector for energy dispersive x-ray analysis (EDX by Oxford Instrument) used for compositional analysis. Measurements were performed at 5 kV for imaging in in-lens mode and at 10 kV for micro-analysis. AFM measurements were performed using a NT-MDT Solver PRO-M microscope with a 100 x 100 μm scanner. UV-VIS optical absorption characterizations were done with a JASCO V670 spectrophotometer in the 300–2500 nm wavelength range.

2 Results and discussion

2.1 Morphological and optical properties

The final structure of the synthesized samples is a hexagonal array of SNS nanounits. The structural parameters of the array as shell thickness, curvature, spacing between adjacent units and size of the units can be controlled by metal deposition and template preparation conditions during the RIE process (total pressure of gas mixture, etching time and initial diameter of the PS nanospheres). A typical morphology is illustrated in Fig. 1b: in this case, the SNS array was obtained with PS nanospheres with initial diameter, $D = 315 \pm 9$ nm, a RIE etching time of 8 minutes and a total metal thickness of about 30 nm (measured on flat films, corresponding to about 20 nm at the nanospheres equator). The resulting final gap between the SNS is of about 120 nm. The RIE process of PS nanospheres is anisotropic because the etching is directed along the normal to the nanospheres plane. Therefore, their final shape is not a sphere but is more similar to a lens.
Each nanounit, the semi-nanoshell, is made by a coverage of Au-Ag alloy on top of the RIE-etched polystyrene nanosphere. The composition of the metallic coverage was checked by EDX spectroscopy, resulting in an atomic concentration of 47% of Ag and 53% of Au. The surface of the SNS presents a very interesting roughness as shown in the FE-SEM image at higher magnification in Fig. 1b. This morphology can be controlled by varying the Ar:O_2 ratio during the RIE process and it is a combined effect of the roughness induced on the etched nanospheres during the RIE process and the sputtering deposition of the metals. The role of the shell roughness on the shape and position of the resonances and on the bulk sensitivity of the sensors was investigated by comparing the results of FEM simulations of Au-Ag SNSA with a flat metallic surface and of SNSA with a rough metallic shell. The results are reported in the ESI†. A uniform random roughness with an amplitude of 20 nm was used in the simulations. This level of roughness corresponds to about 50% of the shell thickness, thus a value comparable to the roughness observed in the experimental samples. Anyhow, differences in the simulated absorbances smaller than 1% between structures with or without roughness were estimated, leading us to conclude that the roughness does not play a crucial role in determining the relevant optical proper-

View Article Online
DOI: 10.1039/C7NR01982C

ties of our system.

The optical properties of the samples can be easily tuned by changing the RIE etching time, which controls the lateral coupling between the SNSs. An example of this effect is shown in Fig. 2, which reports the far-field absorbance spectrum of the SNSA with a gap of 120 nm (blue line, RIE 8 min) and of 35 nm (black line, RIE 3 min). The wavelength of the LSPR peak is $\lambda = 1212$ nm for the RIE 3' sample (black line, high-interaction or HI sample) and it is red-shifted with respect to the one of the RIE 8' sample ($\lambda = 920$ nm, blue line, low-interaction or LI sample), due to the larger lateral coupling between neighboring SNSs.

2.2 Bio-functionalization and LSPR response

To study the application of SNSA as plasmonic biosensors, the samples were functionalized with a typical receptor-ligand couple of biomolecules such as Biotin-Streptavidin. Streptavidin (SA) is a bacterial tetrameric protein from Streptomyces avidinii, with a molecular weight of 60 kDa. Biotin (vitamin H) is a small water soluble molecule with a molecular weight of 244.2 Da. The interaction between Biotin and Streptavidin is characterized in solution by a very high affinity constant ($K_a \cong 10^{13}$ M^{-1}). In particular, four molecules of Biotin can bind to one molecule of Streptavidin in equivalent sites, which are situated on opposite sides of Streptavidin, as sketched in Fig. 1c[35,36]. The high affinity stems from hydrophobic interactions, shape complementarity, hydrogen bonds and structural rearrangement of the protein[36].

The bio-functionalization protocol used for SNS arrays has been extensively investigated in previous works by Van Duyne's group[33]. This protocol is characterized by three steps of functionalization and at each step a different layer of molecules is immobilized on the surface of the samples, as previously described. The SAM of 1-OCT:11-MUA (in 3:1 ratio) forms a protective layer from non-specific interactions, and it allows to bind Biotin on SNSs by a cross-linking reaction with EDC. The receptor layer is not uniform because the Biotin can bind only to the 11-MUA. This is an important aspect because the interaction is influenced by the steric hindrance and by the concentration of biotinylated molecules. At each functionalization step, additional layers of molecules are deposited on the surface, producing a red-shift of the LSPR peak. Since upon functionalization the modification of the absorption curve is not simply a rigid shift but involves both a shift and a deformation, a simple evaluation of the maximum position can be unsatisfactory to follow the dynamic of the biorecognition. Therefore, for the analysis of the LSPR peak shift we monitored the evolution of its centroid, performing at each step a weighted average over the absorbance of the peak abscissas above a given threshold A_{th}, using the following equation:

$$\lambda_{centroid} = \frac{\sum_i \lambda_i \cdot (A_i - A_{th})}{\sum_i (A_i - A_{th})}, \quad (1)$$

where A_i is the absorbance value at wavelength λ_i. The error on the shifts has been evaluated as 3σ (σ being the standard deviation of the centroid in a set of repeated measurements), to take into account both the statistical errors and the errors due to intra-sample inhomogeneities.

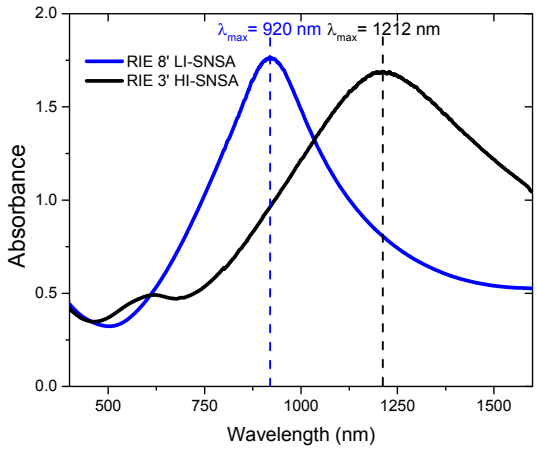

Fig. 2 LSPR spectra for low-interaction (LI) and high-interaction (HI) Au-Ag SNS arrays: absorbance measurements of samples obtained with a RIE etching time of 8 min (blue line, LI) and 3 minutes (black line, HI), respectively.

In order to verify that no modifications of the nanostructures occurred during the bio-functionalization process, the absorbance spectra of several samples were measured before and after the exposure to the PBS solution and successive rinsing and drying. In all the cases, no changes in the spectra were observed. Moreover, the morphological stability of the SNS arrays was checked by FE-SEM measurements of the functionalized samples. The possible oxidation effect of the metallic shells, which might induce a degradation of the sensor performances, thus compromising their stability over time, was taken into account too. To do this, Au-Ag alloy films were deposited by magnetron sputtering during the SNSA synthesis and their optical constants were measured by ellipsometry before and after thermal annealing at 300°C in air (Fig. S5 of ESI†). No variation in the dielectric function was detected.

The response of the LSPR sensors is controlled by the morphological and compositional characteristics of the nanoparticles used, as they define the spectral width, the decay length of the electromagnetic field and the extinction intensity of the spectrum. In this study we have investigated two sets of samples, which differ in size and gap distance between the SNS therefore providing a different level of interaction. In the first case (sample LI), the SNS exhibit a larger gap (about 120 nm) with a lower degree interaction: each SNS can be considered, to a good level of approximation, as an individual sensor. In the other case (sample HI), the SNS have an average gap of about 35 nm, so they can be considered electromagnetically coupled with a higher degree of interaction. The two sets of samples were functionalized with biological molecules and the LSPR response was monitored. For each step of bio-molecules incubation, an incremental red-shift ($\Delta\lambda_c$) of the LSPR peak centroid was observed, as shown in Fig. 3b and c for the low-interaction SNSA (LI-SNSA) and high-interaction (HI-SNSA) samples, respectively. In the case of LI-SNSA, at the first step of functionalization with SAM, the samples exhibit a $\Delta\lambda_c$ of +11 nm, considering a threshold at 50% of the peak height (see Fig. 3a). After the functionalization with Biotin, the samples exhibited an additional red-shift of 5 nm, indicating

View Article Online
DOI: 10.1039/C7NR01982C

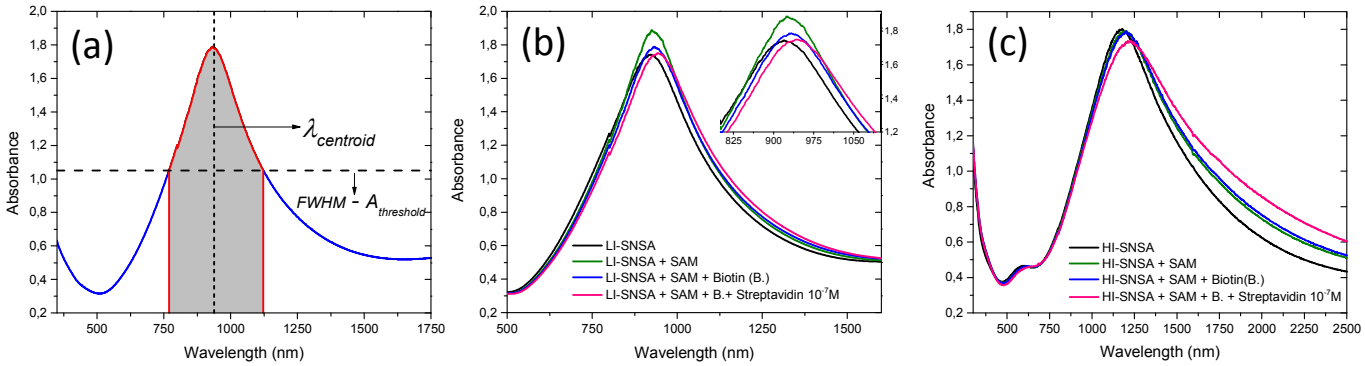

Fig. 3 (a) Schematic illustration of the analysis used for LSPR peaks: $\lambda_{centroid}$ (λ_c) is the centroid of the peak calculated for the part of the spectrum above the threshold A_{th}, according to Eq. 1. (b)LSPR spectra for a sample of LI Au-Ag SNS arrays before and after functionalization with bio-molecules (the λ_c values were calculated choosing a threshold at the value of absorbance (A_{th}) at the 50% of the peak height): λ_c of the sample as deposited (black line) is 923 nm; λ_c after functionalization with SAM is 934 nm (green line); λ_c after functionalization with Biotin is 939 nm (blue line); λ_c after exposition of 100 nM of Streptavidin is 950 nm (pink line). (c) LSPR spectra for a sample of HI Au-Ag SNS arrays functionalized with biological molecules: λ_c of the sample as deposited (black line) is 1204 nm; λ_c after functionalization with SAM is 1230 nm (green line); λ_c after functionalization with Biotin is 1239 nm (blue line); λ_c after exposition of 100 nM of Streptavidin is 1277 nm (pink line).

the successful binding of the receptor. Exposure of the SNSA to 100 nM of Streptavidin results in a maximum $\Delta\lambda_c$ of about +11 nm, corresponding to a saturation of SA for this density of receptors. In the case of HI-SNSA, the samples exhibit a $\Delta\lambda_c$ of +26 nm with SAM, an additional red-shift of 9 nm with Biotin and the exposure of the HI-SNSA to 100 nM of Streptavidin results in a maximum $\Delta\lambda_c$ of about +38 nm. All the LSPR centroid variations were measured considering a threshold at 50% of the peak height.

The LSPR response curve, defined as $\Delta\lambda_c$ as a function of the Streptavidin concentration [SA], was measured in the range 10^{-13} M $\leq$ [SA] $\leq 10^{-6}$ M and the results are shown in Fig. 4. The data were fitted with the model of Langmuir isotherm,[12] according to Eq. 2:

$$\Delta\lambda_c = \Delta\lambda_{c,sat}\frac{K_{a,eff}\cdot[SA]}{1+K_{a,eff}\cdot[SA]}, \qquad (2)$$

where $\Delta\lambda_{c,sat}$ is the saturation value of $\Delta\lambda_c$ and $K_{a,eff}$ is the "effective affinity constant" at the interface. $K_{a,eff}$ and the limit of detection (LOD) of the system under study can be measured from the response curve. In this case the LOD is estimated as the abscissa of the intersection point between the confidence interval associated with the non-response point and the sensing curve, as shown in Fig. 4. For the LI-SNSA, the experimental results have shown $K_{a,eff}$ = (1.0 ± 0.5)×10^9 M^{-1}, a saturation value $\Delta\lambda_{csat}$ = 10 ± 1 nm and a LOD = 2×10^{-10} M. Whereas for the interacting case (HI-SNSA) the results are: $K_{a,eff}$=(3.3 ± 0.5)×10^9 M^{-1}, $\Delta\lambda_{c,sat}$ = 36 ± 1 nm and a LOD = 3×10^{-11}M. A comment is worth to be done at this point. Considering the exposed surface per unit cell of the array of semi-nanoshells, the HI array has a metal surface equal to about 2 times the surface in the LI array. In principle, thus, the HI configuration, that exposes a larger surface to the bio-molecules, should require a larger amount of analyte to be fully covered, and may result to be less sensitive and to have a higher LOD with respect to the LI-SNSA. In fact, only the portion of the shells that is close to the equator (and thus experiences the maximum interaction) participates in the sensing process, leaving a large portion of the metallic surface unused. On the contrary, the experimental results demonstrated that the HI configuration performs better than the LI one, thus further confirming the great importance of the interaction in controlling the performances of the SNSA sensors, which is able to compensate this intrinsic limit of the HI-SNSA.

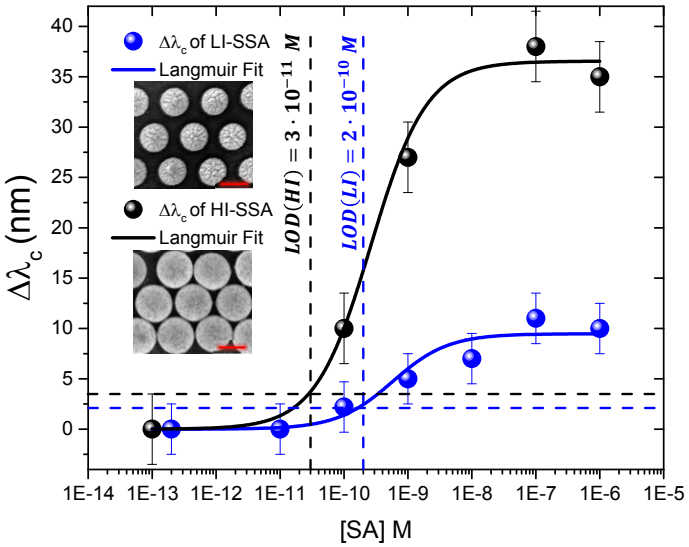

Fig. 4 Measured response curves of $\Delta\lambda_c$ versus [SA] for the binding of SA to a biotinylated SNSs surface for the LI and HI samples. The solid line is the calculated value of $\Delta\lambda_c$ using Langmuir Isotherm described in equation 2. Inset: FE-SEM image of LI- and HI-SNSA samples. The scale bars are 200 nm in both images.

The similar values of $K_{a,eff}$ obtained for HI- and LI-SNSA indicate that the Biotin-Streptavidin interaction is not largely affected by the degree of coupling between SNS, but is mainly controlled by the SNS morphology. As expected, the measured $K_{a,eff.}$ is lower than the value of K_a referred to binding events in solution, and this can be ascribed to the different constraints imposed by the

View Article Online
DOI: 10.1039/C7NR01982C

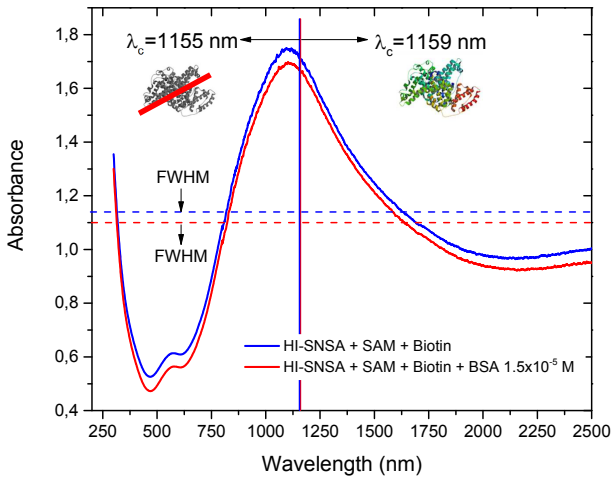

Fig. 5 LSPR spectra for a sample of HI Au-Ag SNS arrays functionalized with bio-molecules: the λ_c at the FWHM of the peak is 1155 nm after functionalization with Biotin (blue line); λ_c at the FWHM after incubation with BSA (1mg/ml)(red line) is 1159 nm.

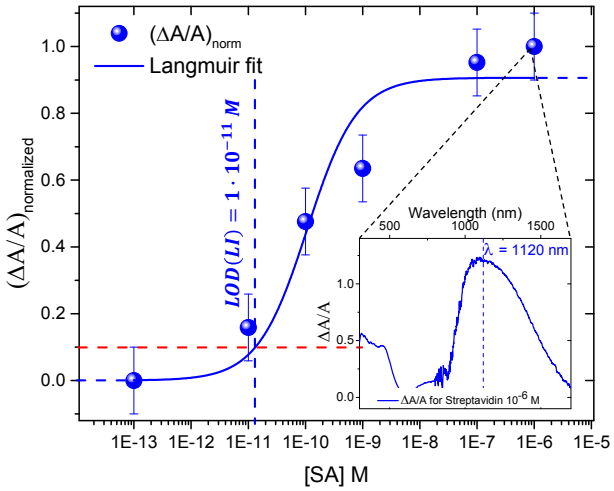

Fig. 6 The normalized ratio ΔA/A in a LI-SNSA versus the Streptavidin molar concentration, [SA], at a fixed wavelength of 1120 nm. The solid line is the calculated value of the normalized ΔA/A using the Langmuir Isotherm. Inset: normalized ΔA/A for the Streptavidin detection at the highest concentration (10^{-6} M) as a function of the wavelength.

solid-liquid interface. In fact, in this configuration the binding is influenced by the concentration and orientation of the ligand and by its interaction with the surface[35]. The LOD obtained with SNSA for Streptavidin is comparable to the value obtained in other works using Au nanoparticles-enhanced SPR sensors[37], confirming the high sensitivity of these systems, which can be further improved by optimizing the functionalization protocol and the structural parameters of the nanoarray.

Another important feature for the development of sensing devices that was investigated in the present work is the sensor sensitivity to an aspecific signal. In order to study the specificity of the LSPR response of the synthesized SNSA and to confirm the protective effect of the thiols layer and of the PEGylated Biotin, the SNSA were functionalized with SAM and Biotin and exposed to a very high concentration of BSA (Albumin from Bovine Serum). BSA is a protein with a molecular weight similar to Streptavidin, and it is usually used to simulate the effect of an interfering species in a biological solution of analytes, such as proteins[33,38]. The typical concentration of BSA used is 1 mg/ml corresponding to a concentration of 1.5×10^{-5} M.
In the present work, a sample of HI-SNSA was tested and the obtained results are shown in Fig. 5. The measured $\Delta\lambda_c$ is +4 nm (i.e., about 10% of $\Delta\lambda_{c,sat}$), using a concentration which is two orders of magnitude higher than the saturation value for Streptavidin. This result indicates that there is not a dramatic effect of aspecific response, in agreement with the results of BSA exposure in Ag nanoprism arrays[33]. Moreover, the SNS arrays are stable after all the chemical treatments and this is confirmed also by the morphological analysis of the functionalized samples. The stability of these systems is very important for the realization of devices, because it is necessary to avoid changes of the LSPR spectra that can be due to alterations of the structure.

2.3 Intensity-interrogation approach

So far, the used approach was based on a wavelength-interrogation mode, i.e., we measured the absorbance at normal incidence by scanning the wavelength of light. We explored also the possibility of using SNSA as an intensity-interrogated biosensor. Therefore, instead of monitoring the LSPR peak centroid shift, we measured the difference in absorbance after exposure to the analyte at a fixed λ. This method is based on the difference between the absorbance values (A) before and after the Streptavidin detection, which can be expressed as in Eq. 3:

$$\left(\frac{\Delta A}{A}\right) = \frac{A_{analyte} - A_{receptor}}{A_{receptor}}. \qquad (3)$$

The major point here is to select the wavelength λ at which the sensor is designed to operate. As a possible criterion, we used the λ corresponding to the maximum point of the $\Delta A/A$ curve for the highest Streptavidin concentration explored (10^{-6} M), where the curve exhibits also the largest stability (i.e., smallest local derivative) as it can be seen in the inset of Fig. 6. Moreover, this λ corresponds approximately to the inflection point of the LSPR spectra after the maximum, which demonstrated to be very sensitive to dielectric environment changes. In this case (LI-SNSA), the wavelength used is 1120 nm and the normalized absorbance ratios were calculated for all the analyte concentrations.

$$\left(\frac{\Delta A}{A}\right)_{norm} = \left(\frac{\Delta A}{A}\right)_{norm,sat} \frac{K_{a,eff}\cdot[SA]}{1+K_{a,eff}\cdot[SA]} \qquad (4)$$

where $(\Delta A/A)_{norm,sat}$ is the saturation value of the $(\Delta A/A)_{norm}$. The fit of these data with the Langmuir isotherm, described by Eq. 4, results in a $K_{a,eff} = (8 \pm 5) \times 10^9$ M^{-1} with a LOD of about 1×10^{-11} M. These results are consistent with those obtained by the centroid analysis and, for the LI-SNSA, indicate that an enhanced LOD can be attained, showing that the SNSA are promising systems also for a fixed wavelength detection scheme.

View Article Online
DOI: 10.1039/C7NR01982C

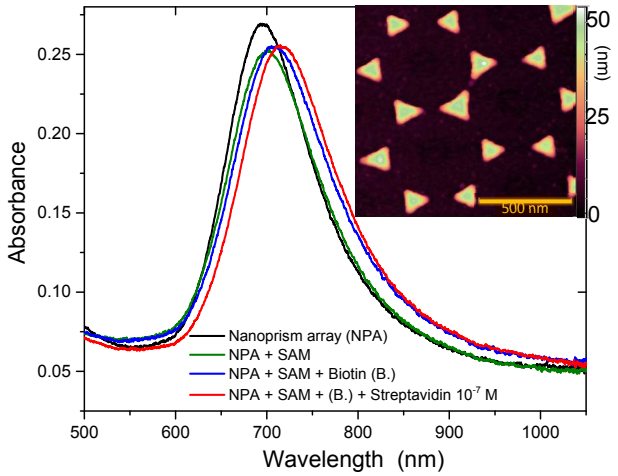

Fig. 7 LSPR spectra for a sample of Ag triangular nanoprisms arrays (NPA) with lateral size L = 116 nm, and height h = 50 nm functionalized with bio-molecules: λ_c of the sample as-deposited (black line) is 695 nm; λ_c after functionalization with SAM is 700 nm (green line); λ_c after functionalization with Biotin is 708 nm (blue line); λ_c after exposition of 100 nM of Streptavidin is 716 nm (red line). Inset: AFM image of a typical sample of Ag triangular NPA.

2.4 Sensitivity comparison with nanoprism arrays (NPA)

We compared the LSPR sensing performances of the bimetallic SNSA with the typical ordered nanostructure that can be synthesized by nanosphere lithography, i.e., the nanoprism array (NPA). Although the shape of these nanostructures and their optical properties are quite different from SNSA, NPA have been studied so extensively during the last years[7,33] that can be considered as a benchmark for NSL-based biosensors. Thus, in the present case we compared the two kinds of nanostructures (SNSA and NPA) that can be obtained starting from the same mask of polystyrene nanospheres, with a lattice parameter $a_0 = 315$ nm. In the NPA, the functional nano-unit is a silver triangular nanoprism obtained by NSL patterning followed by thermal evaporation of the metal[30,33,39,40]. In our case, the nanoprisms have a lateral size $L = 116 \pm 5$ nm and a height $h = 50 \pm 5$ nm.

For the functionalization, we used the same protocol as in the study of SNSA. The LSPR peak of the NPA is around 700 nm, as showed in Fig. 7, and it gets red-shifted after each step of the functionalization protocol as a result of the successful binding of the molecules. Using the centroid method previously described, we obtained the λ_c at each step: after functionalization with SAM, λ_c is shifted of $+5 \pm 1$ nm, after Biotin of $+8 \pm 1$ nm and after exposure to 100 nM of Streptavidin of $+8 \pm 1$ nm. LI-SNSA gave comparable results as NPA, even if NPA nanoprisms were made of Ag whereas SNSA are a Au-Ag alloy. Moreover, HI-SNSA provided better performances in terms of a higher saturation shift, thus demonstrating that SNSA constitute a very interesting nanoarchitecture for LSPR-based bio-sensing of thin molecules layers.

We interpreted these results by comparing the bulk sensitivity $S_{bulk} = \partial\lambda_c/\partial n$ of SNSA and NPA. To this aim, we measured the change in the LSPR centroid with the samples in water (n=1.33) for the Ag NPA and in Norland Optical Adhesive 61 (NOA 61) (n = 1.54) for the HI-SNSA, with respect to air ($n = 1$), i.e., in the first case for a $\Delta n = 0.33$, RIU whereas in the second for a $\Delta n = 0.54$ RIU variation. We have obtained a bulk sensitivity of $S_{bulk}^{(NPA)} = 250 \pm 10$ nm/RIU, while for SNSA a value of $S_{bulk}^{(SNSA)} = 405 \pm 10$ nm/RIU. The experimental absorbance spectra of the two nanoarrays (HI-SNSA and NPA) measured in the different dielectric environment are reported in the ESI†. For Ag NPA, values ranging from 200 nm/RIU to 260 nm/RIU have been reported in literature[39,41], in perfect agreement with our results. It is worth noting that in order to have exactly the same exposed metal surface of the HI-SNSA (but keeping constant the shape of the nanoprisms), a NPA with lattice parameter a_0 of 620 nm, nanoprism side length L of 228 nm and height h of 98 nm should be considered. However, we have recently demonstrated by FEM simulations[39] that such a Ag NPA would have an expected theoretical bulk sensitivity of about 325 nm/RIU, that is, still lower than the value measured for HI-SNSA.

Table 1 Bulk and surface sensitivities for the three investigated nanostructures: $\Delta\lambda_c$ is the redshift of the plasmonic resonance upon exposure to [SA] = 10^{-7} M.

	S_{bulk} [nm/RIU]	$\Delta\lambda_c$ [nm]
LI-SNSA	385	8
HI-SNSA	405	37
NPA	250	8

A final comparison of the absolute local sensitivity among the three investigated nanostructures (LI-SNSA, HI-SNSA and NPA) can be done by comparing the absolute value of the centroid shift, $\Delta\lambda_c$, measured by exposing the three biosensors to the same concentration of Streptavidin [SA] = 10^{-7} M (i.e., at saturation). Since we used the same protocol for the functionalization of the three nanostructures, we can consistently consider $\Delta\lambda_c$ as a quantity directly proportional to their actual local sensitivity S_0. The bulk sensitivity S_{bulk} and $\Delta\lambda_c$ values are summarized in Table 1 for the three investigated nanostructures. The same $\Delta\lambda_c$ was obtained for LI-SNSA and NPA, in spite of the lower bulk sensitivity of NPA. This can be explained considering that, as reported in Ref. [39], the local sensitivity is directly proportional to the bulk sensitivity and inversely proportional to the decay length of the electromagnetic field, and a shorter effective decay length was determined by FEM simulations for NPA than LI-SNSA. Moreover, the data in Table 1 demonstrate that the HI-SNSA system can be more sensitive than Ag NPA made starting from the same PS nanosphere mask, both from the viewpoint of bulk and local sensitivities, even taking into account the fact that SNSA are not made of pure Ag but of an Au-Ag alloy, which has enhanced chemical stability with respect to the pure silver case[42].

3 Conclusions

We synthesized ordered arrays of Au-Ag alloy semi-nanoshells (SNS) with tunable plasmonic properties in the NIR range by combining nanosphere lithography and reactive-ion etching. By controlling the gap distance between the SNS, we have compared the label-free biosensing properties of low-interaction (LI)

View Article Online
DOI: 10.1039/C7NR01982C

and high-interaction (HI) arrays of SNS using a model system of probe-analyte couple, like Biotin-Streptavidin. The LOD obtained for the Streptavidin molecule is of the order of 10^{-11} M and 10^{-10} M for the high-interaction and low-interaction SNSA, respectively, demonstrating the high sensitivity of these systems, which could be further improved by increasing the level of SNS interaction. The SNSA biosensors exhibited a remarkable immunity against aspecific interaction upon exposure to very high concentrations of BSA. An analysis of the performances of the SNSA also in an intensity-interrogation scheme was performed, indicating that the LOD obtained with the low-interaction SNS can be improved with an alternative approach based on the analysis of the absorbance variation measured at a fixed wavelength.

Finally, we have compared the biosensing bulk and surface sensitivity of the Au-Ag alloy SNSA with those of Ag NPA, which are more commonly used as plasmonic sensors. The saturation response of the LI-SNSA is comparable with the results obtained with the NPA, while the interacting HI-SNSA showed a higher signal in agreement with their enhanced bulk and local sensitivity. The experimental bulk sensitivity of the Au-Ag SNSA is much higher with respect to the Ag NPA in good agreement with the FEM calculations. This demonstrates that a label-free biosensing scheme based on bimetallic SNSA improves under many aspects, and in particular in terms of bulk and surface sensing performances, with respect to the currently established NPA-based techniques. Thus the proposed method can be considered as a very promising approach to label-free biosensing, which can be both scaled down to relatively small molecular weight molecules and used as well for larger structures like, for example, viruses or bacteria.

Acknowledgements

This work has been supported by MIUR and University of Padova, Italy, within the Strategic Project PLATFORMS (Grant STPD089KSC) and the Project BINDER (Grant CPDA153538).

References

1 J. Homola, *Chemical Reviews*, 2008, **108**, 462–493.
2 O. Lazcka, F. J. D. Campo and F. X. Muñoz, *Biosensors and Bioelectronics*, 2007, **22**, 1205–1217.
3 K. Gobi, H. Tanaka, Y. Shoyama and N. Miura, *Biosensors and Bioelectronics*, 2004, **20**, 350–357.
4 G. A. Besselink, R. P. Kooyman, P. J. van Os, G. H. Engbers and R. B. Schasfoort, *Analytical Biochemistry*, 2004, **333**, 165–173.
5 P. P. Dillon, S. J. Daly, B. M. Manning and R. O'Kennedy, *Biosensors and Bioelectronics*, 2003, **18**, 217–227.
6 B.-K. Oh, Y.-K. Kim, W. Lee, Y. M. Bae, W. H. Lee and J.-W. Choi, *Biosensors and Bioelectronics*, 2003, **18**, 605–611.
7 J. N. Anker, W. P. Hall, O. Lyandres, N. C. Shah, J. Zhao and R. P. Van Duyne, *Nature Materials*, 2008, **7**, 442–453.
8 W. P. Hall, S. N. Ngatia and R. P. Van Duyne, *The Journal of Physical Chemistry C*, 2011, **115**, 1410–1414.
9 P. Dong, Y. Lin, J. Deng and J. Di, *ACS Applied Materials & Interfaces*, 2013, **5**, 2392–2399.
10 J. Wang, D. Song, L. Wang, H. Zhang, H. Zhang and Y. Sun, *Sensors and Actuators B: Chemical*, 2011, **157**, 547–553.
11 M. Cottat, N. Thioune, A. Gabudean, N. Lidgi-Guigui, M. Focsan, S. Astilean and M. Lamy de la Chapelle, *Plasmonics*, 2012, **8**, 699–704.
12 A. J. Haes, D. A. Stuart, S. Nie and R. P. Van Duyne, *Journal of Fluorescence*, 2004, **14**, 355–367.
13 Y. Lu, G. L. Liu, J. Kim, Y. X. Mejia and L. P. Lee, *Nano Lett.*, 2004, **5**, 119–124.
14 A. Merkoçi, *Biosensors and Bioelectronics*, 2010, **26**, 1164–1177.
15 P. D. Howes, R. Chandrawati and M. M. Stevens, *Science*, 2014, **346**, 1247390–1247390.
16 N. Michieli, R. Pilot, V. Russo, C. Scian, F. Todescato, R. Signorini, S. Agnoli, T. Cesca, R. Bozio and G. Mattei, *RSC Advances*, 2017, **7**, 369–378.
17 M. D. Baaske, M. R. Foreman and F. Vollmer, *Nat Nano*, 2014, **9**, 933–939.
18 X. Cao, Y. Ye and S. Liu, *Analytical Biochemistry*, 2011, **417**, 1–16.
19 X. Liu, B. Choi, N. Gozubenli and P. Jiang, *Journal of Colloid and Interface Science*, 2013, **409**, 52–58.
20 L. Niu, K. Cheng, Y. Wu, T. Wang, Q. Shi, D. Liu and Z. Du, *Biosensors and Bioelectronics*, 2013, **50**, 137–142.
21 J. C. Hulteen and R. P. Van Duyne, *Journal of Vacuum Science & Technology A: Vacuum, Surfaces, and Films*, 1995, **13**, 1553–1558.
22 G. Liu, Y. Li, G. Duan, J. Wang, C. Liang and W. Cai, *ACS Applied Materials & Interfaces*, 2012, **4**, 1–5.
23 C. Wang, W. Ruan, N. Ji, W. Ji, S. Lv, C. Zhao and B. Zhao, *The Journal of Physical Chemistry C*, 2010, **114**, 2886–2890.
24 H. Wang, J. Kundu and N. Halas, *Angewandte Chemie International Edition*, 2007, **46**, 9040–9044.
25 H. Zhang, D. Song, S. Gao, H. Zhang, J. Zhang and Y. Sun, *Talanta*, 2013, **115**, 857–862.
26 H. Zhang, Y. Sun, J. Wang, J. Zhang, H. Zhang, H. Zhou and D. Song, *Biosensors and Bioelectronics*, 2012, **34**, 137–143.
27 Y. Oh, W. Lee, Y. Kim and D. Kim, *Biosensors and Bioelectronics*, 2014, **51**, 401–407.
28 J.-H. Lee, B.-C. Kim, B.-K. Oh and J.-W. Choi, *Nanomedicine: Nanotechnology, Biology and Medicine*, 2013, **9**, 1018–1026.
29 G. Perotto, V. Bello, T. Cesca, G. Mattei, P. Mazzoldi, G. Pellegrini and C. Scian, *Nuclear Instruments and Methods in Physics Research Section B: Beam Interactions with Materials and Atoms*, 2010, **268**, 3211–3214.
30 T. Cesca, N. Michieli, B. Kalinic, A. Sánchez-Espinoza, M. Rattin, V. Russo, V. Mattarello, C. Scian, P. Mazzoldi and G. Mattei, *Nanoscale*, 2015, **7**, 12411–12418.
31 X. Li, H. Hu, D. Li, Z. Shen, Q. Xiong, S. Li and H. J. Fan, *ACS Applied Materials & Interfaces*, 2012, **4**, 2180–2185.
32 M. Larguinho and P. V. Baptista, *Journal of Proteomics*, 2012, **75**, 2811–2823.
33 A. J. Haes and R. P. Van Duyne, *Journal of the American Chemical Society*, 2002, **124**, 10596–10604.

View Article Online
DOI: 10.1039/C7NR01982C

34 D. Samanta and A. Sarkar, *Chemical Society Reviews*, 2011, **40**, 2567–2592.

35 V. H. Pérez-Luna, M. J. O'Brien, K. A. Opperman, P. D. Hampton, G. P. López, L. A. Klumb and P. S. Stayton, *Journal of the American Chemical Society*, 1999, **121**, 6469–6478.

36 L. S. Jung, K. E. Nelson, P. S. Stayton and C. T. Campbell, *Langmuir*, 2000, **16**, 9421–9432.

37 S. Zeng, D. Baillargeat, H.-P. Ho and K.-T. Yong, *Chemical Society Reviews*, 2014, **43**, 3426.

38 K. Hirayama, S. Akashi, M. Furuya and K. Fukuhara, *Biochemical and Biophysical Research Communications*, 1990, **173**, 639–646.

39 N. Michieli, B. Kalinic, C. Scian, T. Cesca and G. Mattei, *Biosensors and Bioelectronics*, 2015, **65**, 346 – 353.

40 L. Brigo, N. Michieli, L. Artiglia, C. Scian, G. A. Rizzi, G. Granozzi, G. Mattei, A. Martucci and G. Brusatin, *ACS Applied Materials & Interfaces*, 2014, 7773–7781.

41 M. D. Malinsky, K. L. Kelly, G. C. Schatz and R. P. Van Duyne, *Journal of the American Chemical Society*, 2001, **123**, 1471–1482.

42 W. Hermoso, T. V. Alves, C. C. de Oliveira, E. G. Moriya, F. R. Ornellas and P. H. Camargo, *Chemical Physics*, 2013, **423**, 142–150.